Electronic Supplementary Material (ESI) for Journal of Materials Chemistry A.

Supporting information

Enhanced thermoelectric performance and high-temperature thermal stability of *p*-type Ag-doped β-Zn_4Sb_3

Lirong Song,[a] Anders B. Blichfeld,[b] Jiawei Zhang,[a] Hidetaka Kasai,[c] and Bo B. Iversen[a,*]

a. Center for Materials Crystallography, Department of Chemistry and iNANO, Aarhus University, DK-8000 Aarhus, Denmark. Email: bo@chem.au.dk

b. Department of Materials Science and Engineering, NTNU Norwegian University of Science and Technology, NO-7491 Trondheim, Norway.

c. Faculty of Pure and Applied Sciences, Tsukuba Research Center for Energy Materials Science (TREMS), University of Tsukuba, 1-1-1 Tennodai, Tsukuba, Ibaraki, 305-8571, Japan.

*E-mail: bo@chem.au.dk

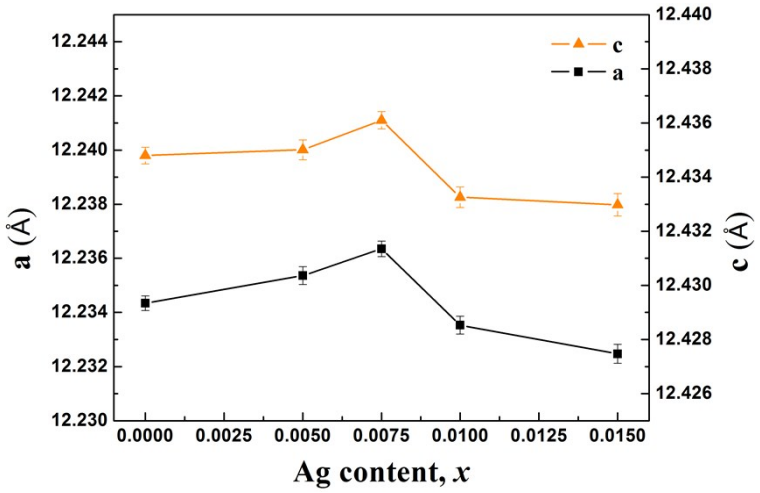

Fig. S1 Lattice parameters a and c of $(Zn_{1-x}Ag_x)_4Sb_3$ as a function of Ag doping content for the top sides of the pellets at RT. The increase in Ag content *x* beyond 0.0075 results in a reduction of lattice parameters, possibly because of the formation of Zn vacancy due to the impurity Ag_5Zn_8, which tends to counterbalance the effect of the difference between ion radii of Ag^+ and Zn^{2+}.

Table S1. Rietveld refinement details of the synchrotron PXRD data at 300 K. (The *R* factors and χ^2 shown here are the data from the main phase, whose weight fraction value is in grey color below.)

Parameters		Zn_4Sb_3		$(Zn_{0.995}Ag_{0.005})_4Sb_3$		$(Zn_{0.99}Ag_{0.01})_4Sb_3$	
T(K)		300-1	300-2	300-1	300-2	300-1	300-2
$t_{exp.}$(min)		15	15	15	15	15	15
No. of points		7930	7931	7931	7933	7935	7934
No. of reflections		3241	452	3268	3470	3230	3463
No. of parameters		51	56	56	56	61	63
R_F (%)		1.68	2.37	1.85	2.77	2.90	2.08
R_{Bragg} (%)		3.12	3.51	3.70	5.26	3.20	3.14
R_p (%)		7.70	11.0	7.48	11.6	8.47	8.17
R_{wp} (%)		8.42	12.0	8.07	14.4	9.05	9.19
χ^2		16.5	56.2	16.0	61.3	16.9	25.0
Wt.% Zn_4Sb_3		94.34(0.19)	-	93.09(0.19)	23.89(0.16)	90.81(0.21)	6.29(0.07)
Wt.% ZnO		4.42(0.06)	45.03(0.20)	5.58(0.08)	8.50(0.12)	5.32(0.10)	12.22(0.08)
Wt.% Sb		1.24(0.03)	44.88(0.15)	1.33(0.03)	-	1.02(0.04)	4.56(0.04)
Wt.% ZnSb		-	10.10(0.09)	-	67.61(0.24)	2.85(0.06)	76.92(0.18)
Zn_4Sb_3	a=b(Å)	12.21951(15)	-	12.21970(12)	12.23696(20)	12.20993(17)	12.22394(34)
	c(Å)	12.40562(16)	-	12.40552(13)	12.43208(25)	12.39731(18)	12.41722(47)
	Biso Sb1	0.762(0)	-	0.771(0)	0.625(0)	0.981(0)	0.477(0)
	Biso Sb2	0.792(0)	-	0.752(0)	1.150(0)	0.954(0)	1.050(0)
	Biso Zn1	1.431(0)	-	1.326(0)	1.790(0)	1.324(0)	1.251(0)
	Volume ($Å^3$)	1604.194(35)	-	1604.231(28)	1612.209(50)	1600.604(40)	1606.859(87)
ZnSb	a(Å)	-	6.20376(15)	-	6.20334(7)	6.20180(68)	6.19815(5)
	b(Å)	-	7.74261(19)	-	7.74292(9)	7.73406(91)	7.73611(6)
	c(Å)	-	8.09745(19)	-	8.09937(10)	8.09277(114)	8.09145(6)
	Biso Zn1	-	0.455(0)	-	0.957(0)	1.500(0)	1.000(0)
	Biso Sb1	-	0.462(0)	-	0.426(0)	1.280(0)	0.412(0)
	Volume ($Å^3$)	-	388.9665	-	389.0283	388.1897	387.9815

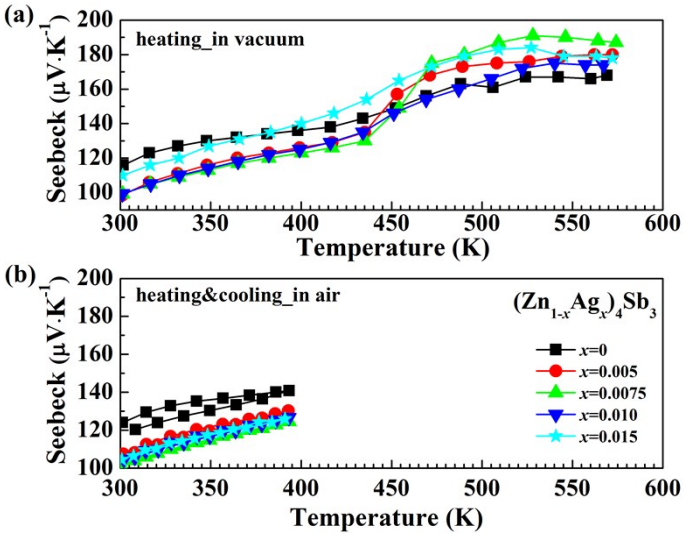

Fig. S2 Temperature dependence of Seebeck coefficient for the $(Zn_{1-x}Ag_x)_4Sb_3$ pellets: (a) heating data measured in vacuum and (b) heating & cooling data measured in air.

Table S2 Sample thickness of $(Zn_{1-x}Ag_x)_4Sb_3$ (x = 0, 0.005, 0.0075, 0.010, 0.015) pellets.

Sample	Thickness(mm)
Zn_4Sb_3	2.016
$(Zn_{0.995}Ag_{0.005})_4Sb_3$	1.970
$(Zn_{0.9925}Ag_{0.0075})_4Sb_3$	2.029
$(Zn_{0.99}Ag_{0.01})_4Sb_3$	1.980
$(Zn_{0.985}Ag_{0.015})_4Sb_3$	2.024

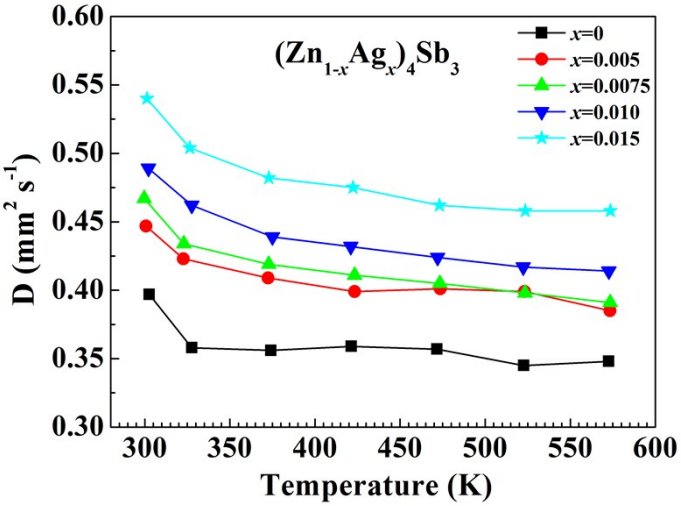

Fig. S3 Temperature dependence of thermal diffusivity measured by LFA for the $(Zn_{1-x}Ag_x)_4Sb_3$ pellets.

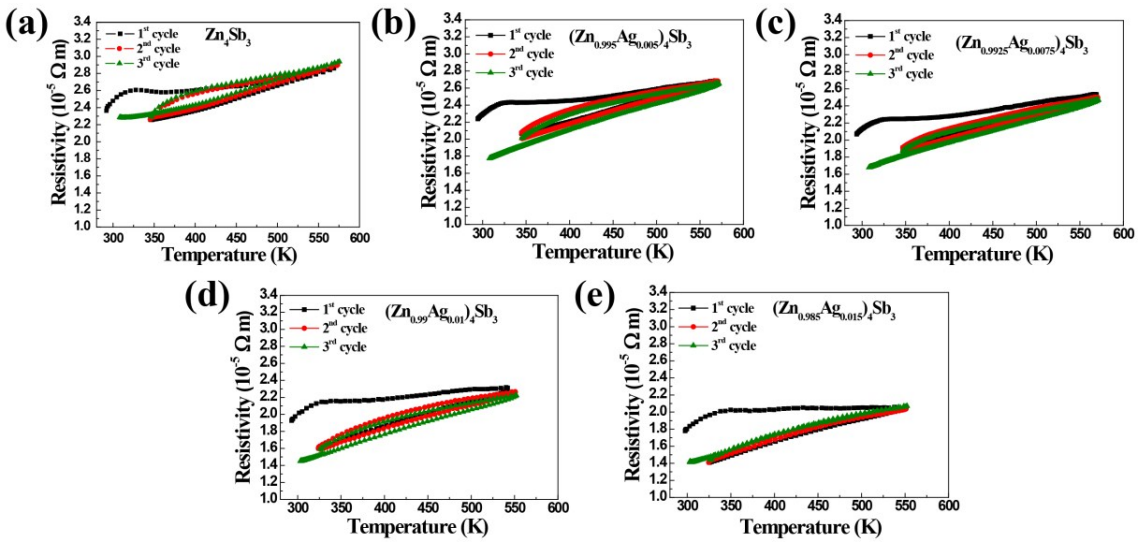

Fig. S4 Temperature dependence of the electrical resistivity for the as-pressed $(Zn_{1-x}Ag_x)_4Sb_3$ pellets in three cycles: (a) x = 0, (b) x = 0.005, (c) x = 0.0075, (d) x = 0.01 and (e) x = 0.015.

Figure S4 shows that as the Ag content increases, the hysteresis loop between the heating and cooling curves becomes smaller and even disappears for the sample with x = 0.015, indicating that Ag doping has an influence on the microstructure change of Zn_4Sb_3 while undergoing the heat treatment.

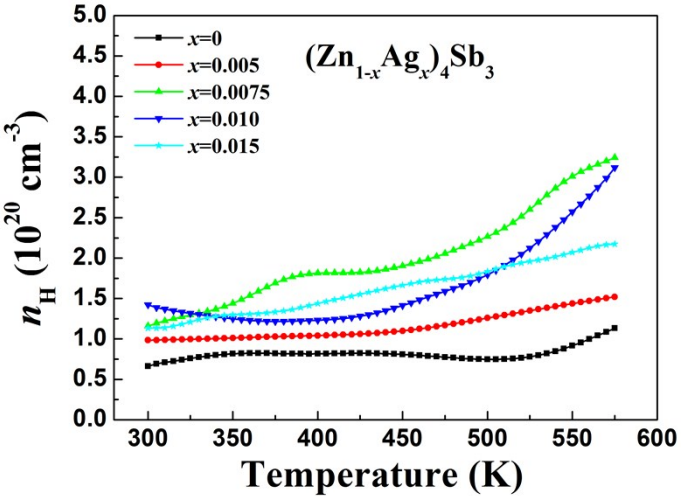

Fig. S5 Temperature dependence of Hall carrier concentration during the cooling segment of the last cycle for the as-pressed $(Zn_{1-x}Ag_x)_4Sb_3$ pellets: (a) x = 0, (b) x = 0.005, (c) x = 0.0075, (d) x = 0.01 and (e) x = 0.015.

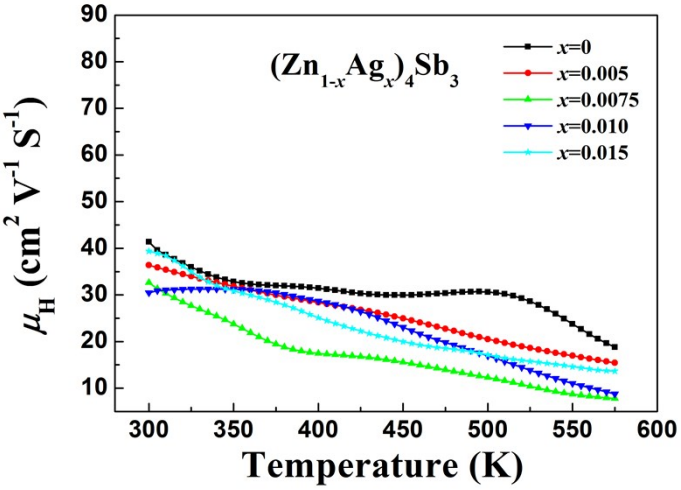

Fig. S6 Temperature dependence of Hall mobility during the cooling segment of the last cycle for the as-pressed $(Zn_{1-x}Ag_x)_4Sb_3$ pellets: (a) x = 0, (b) x = 0.005, (c) x = 0.0075, (d) x = 0.01 and (e) x = 0.015.

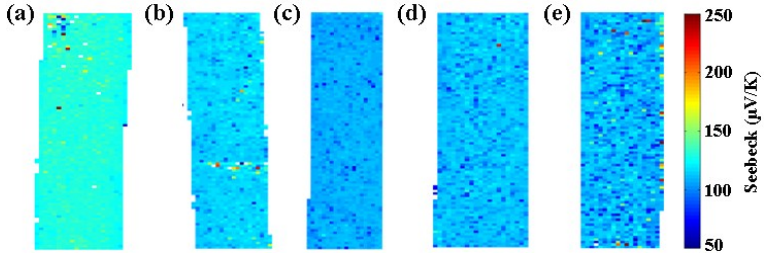

Fig. S7 Room temperature PSM scanning images of the cross sections for $(Zn_{1-x}Ag_x)_4Sb_3$ pellets after the property measurements: (a) x = 0, (b) x = 0.005, (c) x = 0.0075, (d) x = 0.01 and (e) x = 0.015.

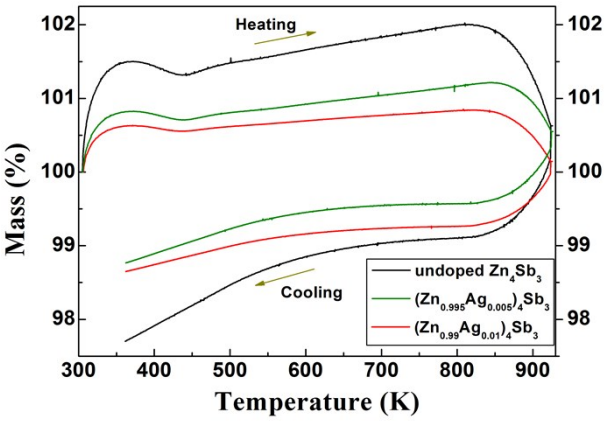

Fig. S8 TG curves of the (a) heating and (b) cooling process for $(Zn_{1-x}Ag_x)_4Sb_3$ (x = 0, 0.005, 0.01) powder samples.

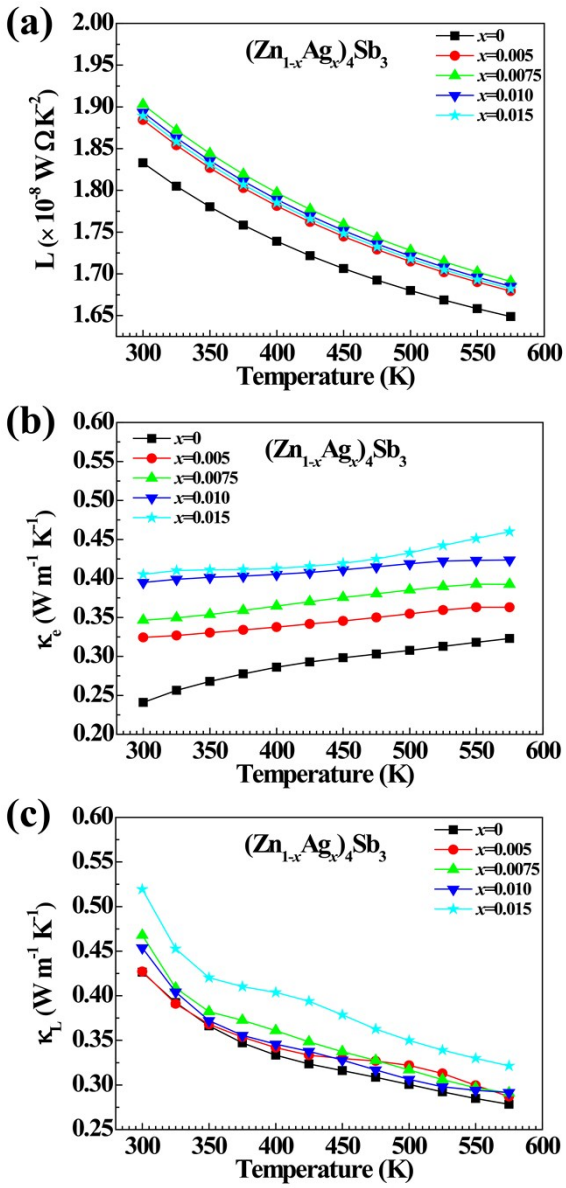

Fig. S9 Temperature dependence of (a) Lorenz number, (b) electronic thermal conductivity and (c) lattice thermal conductivity for the $(Zn_{1-x}Ag_x)_4Sb_3$ pellets. The lattice thermal conductivity κ_L is calculated by subtracting the electronic contribution κ_e from the total thermal conductivity κ, while κ_e is estimated by the Wiedemann-Franz relation $\kappa_e = L\sigma T$, where the Lorenz number L is determined by a single parabolic band model assuming acoustic phonon scattering.